

DYNAMIC BEHAVIOR OF FOUNDATION FOR STEEL POST OF ROCKFALL PROTECTION FENCE UNDER IMPACT LOADING

S. KONDO*, M. KOMURO, N. KISHI and Y. YAMAMOTO

Graduate School, Muroran Institute of Technology, Muroran, 050-08585, Japan

Emails: s.kondo-i@sunagonet.co.jp, komuro@mmm.muroran-it.ac.jp, kishi@mmm.muroran-it.ac.jp,
yamamoto@sunagonet.co.jp

*Corresponding author

Abstract. *In order to investigate the dynamic behavior of the steel posts of a rockfall protection fence embedded into a concrete (RC) retaining wall, static and drop-weight impact loading tests were conducted on 100 cm long H-section posts installed into the plain concrete foundation model. In these tests, a 300 kg steel weight was used and was dropped from a predetermined height. In these tests the specimen was changed for each test. The results obtained from this study are as follows: 1) a plastic hinge was formed near the base of the foundation in both cases of static and impact loading; and 2) based on the strain distributions in the post model, the anchoring depth of the post may be larger than that from design specification.*

Keywords: steel posts of rockfall protection fence; impact loading; anchoring depth; plastic hinge

1. INTRODUCTION

In Japan nowadays, the development of residential land has been extended close to steep slopes and road networks have also been constructed along cliffs and slopes. However, mudflows and other severe natural disasters have sometimes occurred in these areas due to torrential rains caused by climate changes in recent years. Usually, many check-dams have been constructed to control mudflows in steep valleys. However, earth and sand were deposited on these dams with the passage of time and, as a result, driftwood and large rocks flow down to the foot of mountains when mudflows occur. In order to restrain such mudflows, protection fences were installed at the tops of the dams.

On the cliff side of roads, rockfall protection fences were installed in the top surface of the rockfall protection retaining wall in order to ensure the safety of transportation networks from the falling rocks as shown in Fig. 1 (Japan River Association, 2017). Generally, the check-dams and rockfall protection retaining walls were designed as gravity-type plain concrete structures. Therefore, the steel posts for supporting the fence were placed in a prepared hole left at the top of the wall and back-filled with the same concrete as in the walls.

At present, these steel posts are designed following the Rockfall Countermeasures Handbook (Japan Road Association, 2017a) (referred to hereinafter as Handbook). But, the dynamic response characteristics of the posts under impact loading due to rock fall, mudflows, and/or similar events have not been accounted for in the Handbook and these impact loads were assumed to act as static loads. However, it was reported that the posts subjected to impact loads due to falling rocks were actually severely damaged as shown in Photo 1 (Civil Corporation

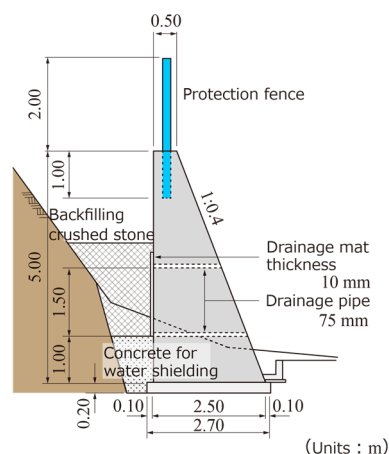


Figure 1. Rockfall protection retaining wall embedded with steel posts for fence.



Photo 1. An example of damaged retaining wall due to falling rocks.

website), in which the concrete walls near the embedded post were spalled. Therefore, in order to ensure greater safety of the transportation networks from falling rocks, it is very important to establish a rational design method for the steel posts of the rockfall protection fences considering the impact-resistant characteristics.

From this point of view, in this study to investigate the dynamic response characteristics of the posts, these impact loading tests on the steel posts supported by embedding one end into the plain concrete block (referred to hereinafter as foundation) was conducted. Here, a static loading test was also carried out for comparison.

2. EXPERIMENTAL OVERVIEW

2.1. Test Specimen and Experimental Method

Figure 2 shows the dimensions of test specimens and rebar arrangement. The foundation models have dimensions of $700 \times 400 \times 1,300$ mm (width \times height \times length), in which a part of 60 cm length from its front surface was taken as the footing for the steel post and the other part as the anchorage of the model. In order to minimize the reinforcing effects of rebars on the load-carrying capacities of the footing, axial rebar and stirrups were placed at the location of 30 cm from the center of the footing in the cross-sectional plane. The diameters of the axial rebar and stirrup were 19 and 10 mm, respectively.

Here, H-section steel members of 100 mm width and height were used for the steel post model, even though members of 100 mm width and 200 mm height H-section posts have been widely used for the actual ones of a conventional rockfall protection fence. However, in this study, the small sized members were used to save size and weight of the foundation models.

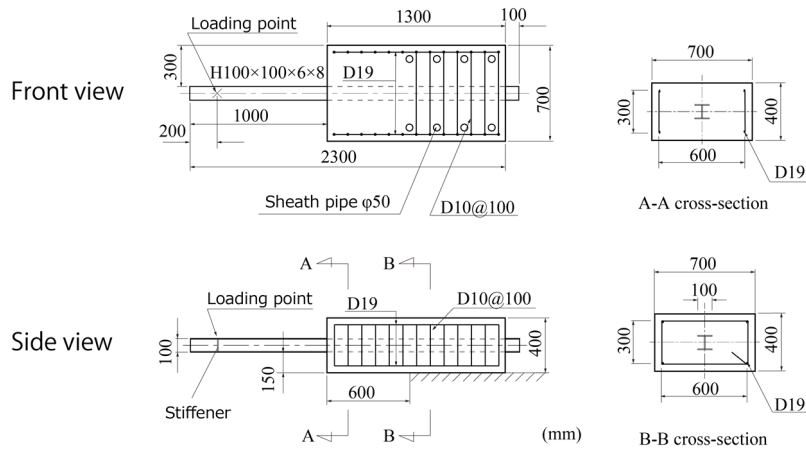


Figure 2. Dimensions of test specimen and rebar arrangement.



Photo 2. View of experimental setup.

The height of the footing may be similar to the depth of the top surface of a conventional retaining wall.

The loading point for the H-section post for static and drop-weight impact tests was 800 mm from the front surface (base) of the footing for bending action to be predominant. The 6 mm thick stiffener plates were welded to the flange and web of the posts at the loading point to restrain these against local buckling.

The foundations were anchored to the rigid steel jig by fastening with bolts and nuts. At the start of the tests, the compressive strength of the concrete f_c was 34.5 N/mm^2 . Also, the yield stress f_y and ultimate strength f_u of the H-section steel posts obtained from the mill sheet were 354 and 449 N/mm^2 , respectively.

In this study, in order to investigate the dynamic response characteristics, the failure behavior of the steel post and footing, and the anchoring depth of the posts, impact loading tests were conducted while varying the drop height of the weight through 4 levels: 0.1; 0.5; 1.0; and 1.5 m, respectively. The tests were conducted following a single loading method, in which a steel weight with a mass of 300 kg and a tip diameter of 200 mm was allowed to drop freely onto the H-section steel post from the prescribed height once only. Here, the static loading test was also conducted for comparisons with the dynamic response characteristics by using a hydraulic jack. Photo 2 shows the test setups for static and drop-weight impact loading.

2.1. Measuring Quantities

Figure 3 shows the measuring points of axial strains of H-section posts and the vertical displacements of the specimens. Strain gauges were glued at 30 mm upper and lower points from the center of the post for a total of 19 sections in the whole span area to investigate the dynamic behavior and anchoring depth of the post.

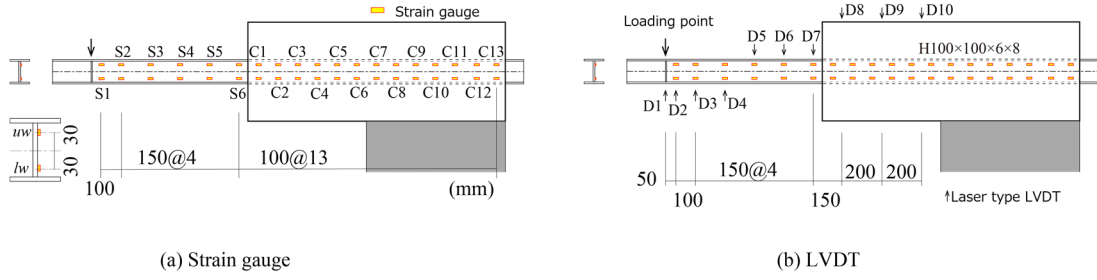


Figure 3. Location of measuring points.

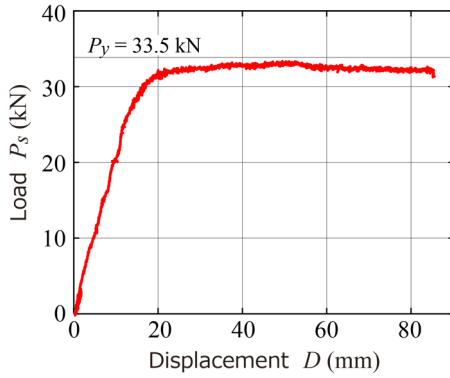


Figure 4. Load-displacement curve under static loading.

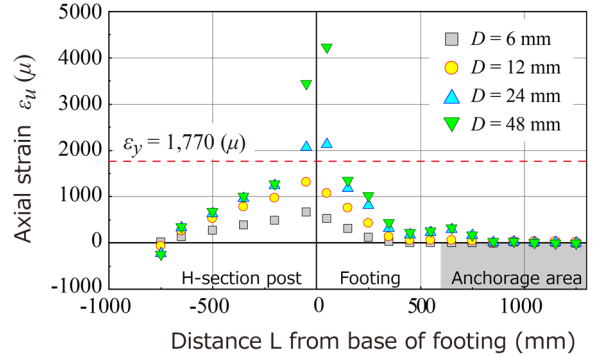


Figure 5. Axial strain distribution at upper fiber of H-section post under static loading.

The vertical displacements of the post and foundation were measured by using a laser-type LVDT. In this paper, displacements of the anchorage area of the foundation were also measured to see whether it was uplifted or not. The impact force generated by the drop weight was measured by using a load cell installed in the weight.

These analog data were converted into digital data and recorded in the digital data recorders with a sampling time of 0.1ms.

3. EXPERIMENTAL RESULTS AND DISCUSSIONS

3.1. Static Loading Tests

Figure 4 shows the load P_s and displacement D at the loading point (referred to hereinafter as displacement) curve obtained from the static loading test. In this figure, the calculated yield load P_y of the H-section post was also indicated which was estimated by using the calculated yield bending moment M_y . From this figure, it is observed that the load P_s almost linearly increased until a displacement D reached around 12 mm, and after that the load gradually increased and then kept constant after the displacement reaching 24 mm. However, the maximum load did not reach the calculated yield load P_y . This may be due to the load being estimated by using a nominal section modulus and the value of the yield stress from the mill sheet.

Figure 5 shows the axial strain distribution ϵ_u at the upper fiber of the H-section post at a displacement reaching some typical values. Here, the upper fiber strains were evaluated based on the plane conservation concept and two measured strain values of ϵ_{uw} and ϵ_{lw} . In this figure, the yield strain ϵ_y of the post was evaluated by using the yield stress obtained from the mill sheet and is also shown.

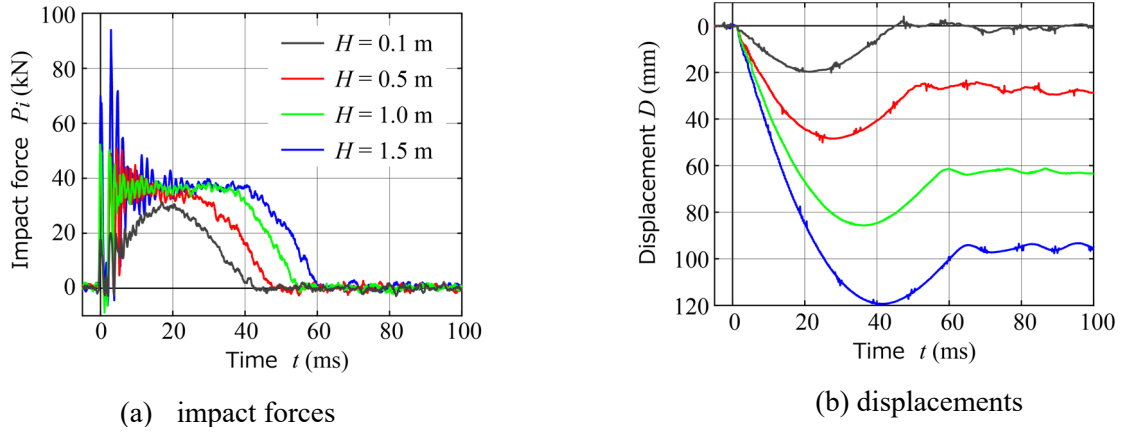


Figure 6. Comparisons of time histories of dynamic responses under impact loading.

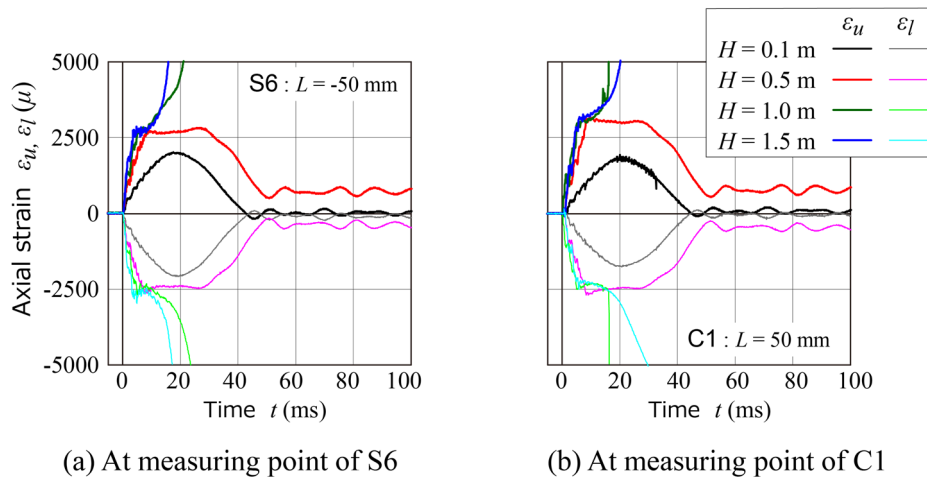


Figure 7. Comparisons of time histories of axial strains in H-section post.

Focusing on the strain distributions in the cases of deflections of $D = 6$ and 12 mm, it is observed that they are linearly distributed from the loading point toward the base of the footing and, on the other hand, the distributions inside of the footing tend to decrease and reached almost zero strain at 450 mm distance from the base of the footing.

In the case of $D = 24$ mm, it is seen that the strains in the H-section post near the base of the footing have exceeded the yield strain and the area was in a yielding state. At $D = 48$ mm, this indicates that only the strains near the base increased and strains in the other regions gave similar values at $D = 24$ mm. This suggests that a plastic hinge may have formed near the base of the footing.

3.2. Impact Loading Tests

Figure 6 shows configurations of the time history of the weight impact force P_i and the displacement D at each drop height of the weight (referred to hereinafter as drop height) H . In these figures, the origin of the time axis was taken as the actual time when the weight impacted the H-section post.

From Fig. 6(a), the following can be observed: (1) time histories of the impact forces P_i were composed of half sine and/or trapezoidal-shaped waves and high-frequency components; and (2) even though the maximum impact forces P_i tend to increase with increasing drop height H , the forces P_i reduced to zero after keeping a constant value around 40 kN for 15 to 30 ms except

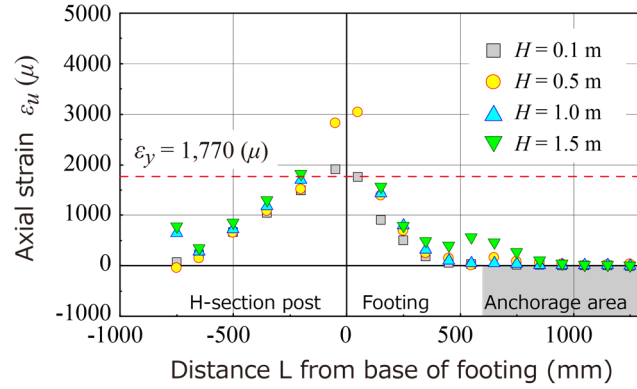


Figure 8. Comparisons of upper fiber strain distribution of H-section post at max. displacement.

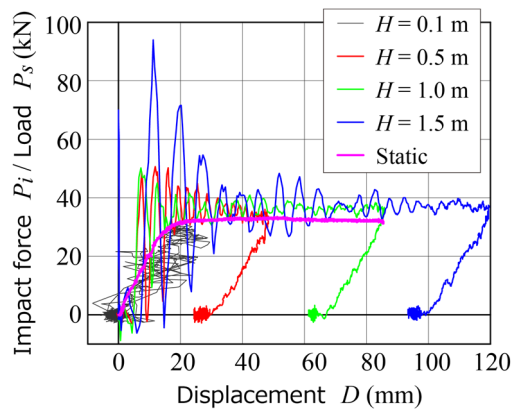


Figure 9. Comparisons of load-displacement curves between static and impact loading.

when the drop height $H = 0.1$ m. Since the constant value of the impact force was approximately same as the plastic load $P_z (= 38.2$ kN) which was estimated assuming perfect elasto-plastic behavior, this may be due to a plastic hinge forming near the base of the footing.

From the experimental results for the drop height $H = 0.1$ m, since the maximum impact force ($P_{i \max} = 31.3$ kN) was smaller than the static maximum load ($P_{s \max} = 33.5$ kN) and the deflection was perfectly restored as shown in Fig. 6(b), the specimen behaved elastically.

From Fig 6(b), these findings indicate that: (1) the maximum displacement tends to increase with increasing drop height H ; and (2) the time passed from the beginning of impact (referred to hereinafter as passed time) on reaching the maximum displacement was similar to that when the impact force decreased.

Figure 7 shows the time histories of the upper and lower fiber strains ε_u and ε_l at the measuring points S6 and C1, which are near the base of the footing. From this figure, it is observed that: (1) if the drop height is $H \leq 0.5$ m, the upper and lower fiber strains were almost symmetrically distributed; however, (2) in the case of a drop height greater than $H = 0.5$ m, the strains were not symmetrically distributed and were considerably greater than the yield strain.

Figure 8 shows the upper fiber strain distributions of the H-section posts at maximum displacement. From this figure, the following details can be observed: (1) in the case of a drop height $H = 0.1$ m, the strains are almost linearly distributed from the loading point to the base of the footing; after that, (2) these gradually decreased inside of the footing and then reached zero strain at the location of 450 mm from the base surface. These distribution characteristics are similar to those within the elastic state at static loading.

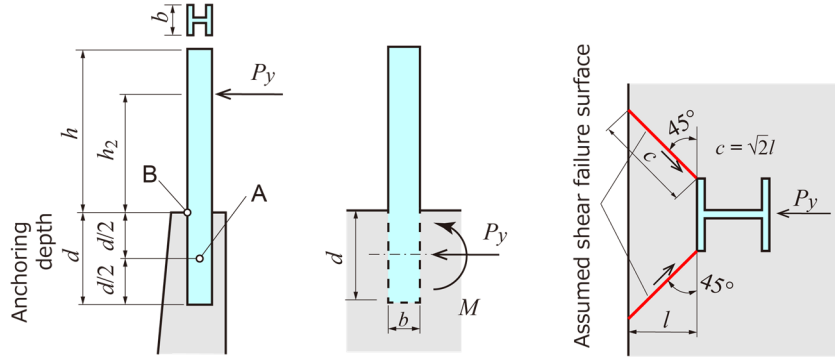


Figure 10 Schematic diagram for designing anchoring depth of fence post.

In the case of a drop height $H = 0.5$ m, the strain of the H-section post near the base of the footing exceeded the yield value. Furthermore, in the cases of $H = 1.0$ and 1.5 m, a plastic hinge may be formed in this area because the strain was greater. On the other hand, each strain of the H-section post excluding the loading point and the area near the base of the footing was almost the same irrespective of the magnitude of the drop height H . This suggests that a plastic hinge was formed near the base of the footing similarly to the static loading case. And also, the strain distribution of the post inside the footing was qualitatively similar to that under static loading.

3.3. Comparisons of Load-Displacement Curves

The impact load P_i and displacement D_i curves under impact loading are shown in Fig. 9 compared to those under static loading. From this figure, it is observed that when the drop height H was equal to or greater than 1.0 m, the curves tend to be similar to that under static loading with increasing displacement. In the case of $H = 0.1$ m, since the curve was almost linearly distributed accompanied by some noise, the post must behave elastically as mentioned above.

3.4. Considerations Concerning the Anchoring Depth of the Post

In the Handbook, for designing the anchoring depth of the post in the footing it is recommended that the bending and punching shear load-carrying capacities of the footing should be checked. In the specification, the bending moment and shear impact force at a point one half of the anchoring depth d of the post in the footing were modeled by considering the anchoring part of the post as a short pillar. In this paper, the anchoring depth d prescribed in the specification will be compared with the experimental results obtained from this study.

The bending compressive stress σ at the base B of the footing (see Fig. 10) was specified so as to be less than the allowable bending compressive stress σ_a of concrete. The stress σ is described as follows:

$$\sigma = \frac{P_y}{A} + \frac{M}{Z} \leq \alpha \sigma_a \quad (1)$$

in which P_y : yield load when a plastic hinge is formed near the base of the post; A: area of flange surface of the post inside the footing ($= bd$); Z: section modulus of the area which is equal to that of the flange of the post ($= bd^2/6$); α : safety factor ($= 1.5$); and M : bending moment at point A shown in Fig. 10. The bending moment M is given as follows:

$$M = P_y \left(h_2 + \frac{d}{2} \right) \quad (2)$$

Where h_2 is a distance from the base to the impacted point of a falling rock; and d is the anchoring depth of the post.

However, the shear stress τ in the wall, obtained by assuming the shear failure surface shown in Fig. 10, is specified to be less than the allowable punching shear stress τ_a . The stress τ is given by the depth of the concrete cover l as follows:

$$\tau = \frac{P_y}{2ld} \leq \alpha\tau_a \quad (3)$$

Here, the allowable bending compressive stress σ_a and the punching shear stress τ_a were estimated following the Specifications for Highway Bridges (Japan Road Association, 2012 and 2017b) as: $\sigma_a = 11.5 \text{ N/mm}^2$; and $\tau_a = 1.09 \text{ N/mm}^2$, respectively.

Estimating the anchoring depths using Eqs. (1) and (3), the following results were obtained: $d_m = 346 \text{ mm}$ and $d_s = 68 \text{ mm}$, respectively, for the bending compressive stress σ and punching shear stress τ . Therefore, the required anchoring depth for design purposes in the case of this test is $d \approx 350 \text{ mm}$.

On the other hand, experimental results for the anchoring depth d_e for static and impact loading are as follows: (1) in the case of static loading, considering the strain distribution of the H-section post at the displacement D reaching 12 mm, d_e was evaluated as $d_{e, st} = 450 \text{ mm}$ (Fig. 5); and (2) in the case of impact loading, the depth $d_{e, i}$ was evaluated as 450 mm at the drop height $H = 0.1 \text{ m}$; however, (3) the depth $d_{e, i}$ may be larger than the value of 450 mm at a higher drop height than $H = 0.1 \text{ m}$ (Fig. 8).

The strain distribution in the post may not be directly compared with the specified anchoring depth determined from the Handbook, because the post model assumes full penetration into the foundation. However, it is confirmed that the anchoring depths of the tests were larger than the design value, but the concrete blocks have not yet debonded from the footing.

4. CONCLUSIONS

In this paper, in order to investigate the dynamic behavior and actual anchoring depth of the posts for protection fences installed into the rockfall protection retaining walls, static and impact loading tests were carried out on the specimens. The specimens were made of an H-section steel post fully penetrated into the foundation model. The results obtained from this study can be summarized as follows:

1. The H-section steel post models reached the ultimate state, forming a plastic hinge near the base of the footing at both static and impact loading; and
2. The anchoring depth of the post in the footing obtained from the experiments may be larger than the specific design value; however, the concrete cover has still not yet debonded from the footing.

REFERENCES

- Civil Corporation website, <https://www.rcnet.co.jp/product/list/listless>. In Japanese
- Japan River Association, (2017), Ministry of Construction Technical Criteria for River Works (Draft), Commentary, Part II Design. *In Japanese*
- Japan Road Association, (2017a), Rockfall Countermeasures Handbook. *In Japanese*
- Japan Road Association, (2012), Specifications for Highway Bridges and Commentary, Part III Concrete Bridges. *In Japanese*
- Japan Road Association, (2017b), Specifications for Highway Bridges and Commentary, Part III Concrete Bridges and Concrete Members. *In Japanese*